

# INHOMOGENEOUS AXIAL DEFORMATION FOR ORTHOPEDIC SURGERY PLANNING

Sergei Azernikov

Siemens Corporate Research, 755 College Road East, Princeton NJ 08540, U.S.A.

**Keywords:** Feature preserving spatial deformation, Weighted arc-length curve parametrization, Orthopedic surgery planning.

**Abstract:** Intuitive global deformation of complex geometries is very important for many applications. In particular, in the biomedical domain, where interactive manipulation of 3D organic shapes is becoming an increasingly common task. Axial deformation is natural and powerful approach for modeling of tubular structures, like bones. With this approach, the embedding space is associated with deformable curve, the handle axis, which guides deformation of the embedded model. As a result, the produced deformation is homogeneous and independent of the model representation and shape. However, in many situations it is beneficial to incorporate geometric and physical properties of the model into the deformation formulation. This leads to *inhomogeneous* axial deformation which allows to achieve more intuitive results with less user interaction. In this work, the inhomogeneous axial deformation is achieved through *deformation distribution function (DDF)* induced on the guiding axis by the embedded model. Since with the proposed formulation the DDF can be pre-computed, run-time computational complexity of the method is similar to the original axial deformation approach.

## 1 INTRODUCTION

Growing amount of available high definition 3D data opens broad opportunities in many different areas. In particular in biomedical domain, increasing number of procedures are planned and executed in computer-aided environment using 3D models of patient's anatomy. Manipulation of these anatomical models, however, often requires new tools and methods, which are not provided in the traditional geometric modeling systems (see for example (Azernikov, 2008)).

One of the earliest yet powerful and intuitive methods for shape manipulation is spatial deformation pioneered by Barr (Barr, 1984). Later, Sederberg and Parry (Sederberg and Parry, 1986) extended the spectrum of possible deformations by introducing the free-form deformation (FFD) approach. Due to its attractive properties and conceptual simplicity this approach was extensively used in geometric modeling and computer animation (Gain and Bechmann, 2008). The basic idea of the FFD approach is to parameterize the embedding space as a tri-variate tensor product volume. The shape of this volume can be manipulated by grid of control points. Once control points are repositioned, the volume is warped and the embe-

dded objects are deformed accordingly. The drawback of the grid-based FFD is that because of the high number of control points that should be moved, it may require significant user interaction even for simple deformations. In order to reduce the amount of required user interaction, lower dimensional variations of the original trivariate FFD method were introduced: surface deformation (Feng et al., 1996) and axial deformation (AxDf) (Lazarus et al., 1994). With the AxDf approach, the ambient space deformation is guided by axial curve, which can be represented as a straight segment chain (Lazarus et al., 1994) or parametric curve (Peng et al., 1997). The major drawback of spatial deformation is that it is global, and as such, does not preserve shape of the local features.

Recently, mesh-based deformation techniques gained popularity in the computer graphics community (Sorkine, 2005; Lipman et al., 2005). These techniques are formulated directly on the polygonal mesh and explicitly designed to preserve local surface features. From the user perspective, with these techniques the deformable object behaves like elastic *homogeneous* material.

Popa et al. (Popa et al., 2006) applied material-aware scheme for mesh deformation assigning stiffness property to various regions of the mesh. As a

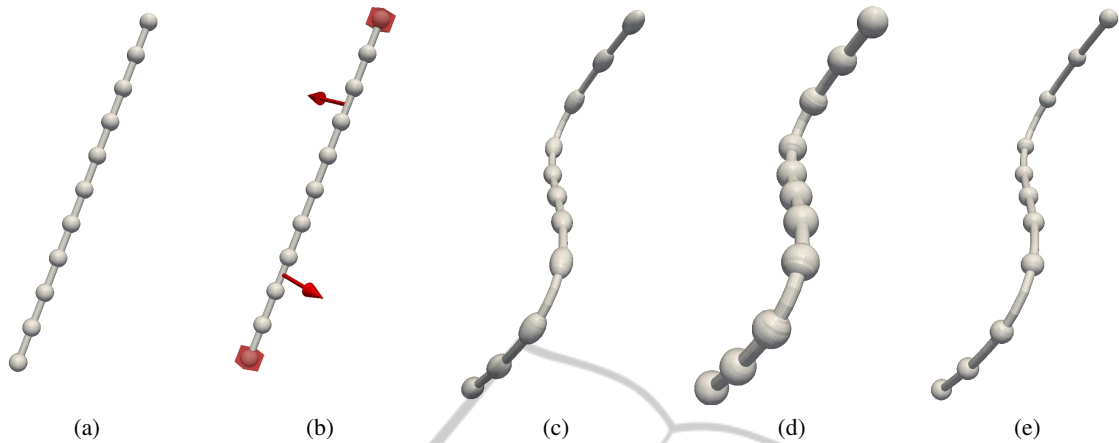


Figure 1: Inhomogeneous axial deformation example: (a) original model, (b) applied deformation and constraints cause stretching, (c) homogeneous axial deformation produces distortion of the spheres, (d) scaling can prevent distortion but modifies size of the spheres, and (e) proposed inhomogeneous axial deformation preserves shape and size of the spheres, while transferring the deformation to cylindrical regions invulnerable to stretching.

result, the deformation is non-uniformly distributed. Kraevoy et al. (Kraevoy et al., 2008) proposed a method for feature-sensitive scaling of 3D shapes. With this approach, the embedding volume is voxelized and scaling function is evaluated in each voxel based on the embedded shape variation. When scaling is applied, the deformation is distributed in a non-uniform manner according to the assigned scaling function values. These methods attempt to mimic behavior of elastic *inhomogeneous* material. The work described in this paper is inspired by this idea and introduces inhomogeneous axial deformation framework.

## 2 INHOMOGENEOUS AXIAL DEFORMATION

When the handle axis length is modified during the modeling session, the aspect ratio of the deformed object is naturally modified as well. Since the deformation is global, the stretching is distributed equally along the axis. Although this behavior is often perfectly desired, it may cause distortion of local features as shown in Figure 1(c). One way to deal with this problem is to scale the model to compensate for the length change. This, however, may lead to non-intuitive results, as can be seen in Figure 1(d). In order to overcome this issue, the *inhomogeneous* axial deformation formulation is proposed in this paper. The basic idea is to redistribute the deformation along the axis such that most of the distortion is applied on invulnerable portions of the model. This behavior attempts to mimic the physical behavior of an inho-

mogeneous bar under axial load (Timoshenko, 1970), which is briefly described in Section 2.1. Based on this analogy, deformation distribution function (DDF) is introduced in Section 2.3. In order to prevent distortion of the model features, the axial curve is reparameterized according to the DDF, as described in Section 2.2. Section 2.5 describes embedding of the model into the axial parametric space. When the axial curve is deformed, its deformation is transferred to the embedded model following the established embedding. The flow chart of the proposed deformation method is shown in Figure 2.

### 2.1 Inhomogeneous Bar Deformation under Axial Load

Let  $B$  be a bar with variable cross section  $A(t)$ ,  $t \in [0, 1]$  and length  $L$ , as shown in Figure 3. The local deformation  $\delta s$  of  $B$  under axial load  $P$  can be computed as (Timoshenko, 1970):

$$\delta s(t) = \int_0^t \frac{P}{E(t)A(t)} dt, \quad (1)$$

where  $E(t)$  is the Young modulus of the bar (Timoshenko, 1970). Introducing stiffness notion  $k(t) = A(t)E(t)$  and assuming constant force  $P = const$ ,

$$\delta s(t) = P \int_0^t k^{-1}(t) dt. \quad (2)$$

Then, the total deformation of the bar is

$$\delta L = P \int_0^1 k^{-1}(t) dt. \quad (3)$$

In the inverse problem, total deformation  $\delta L$  of the bar is given, when local deformation and stress should

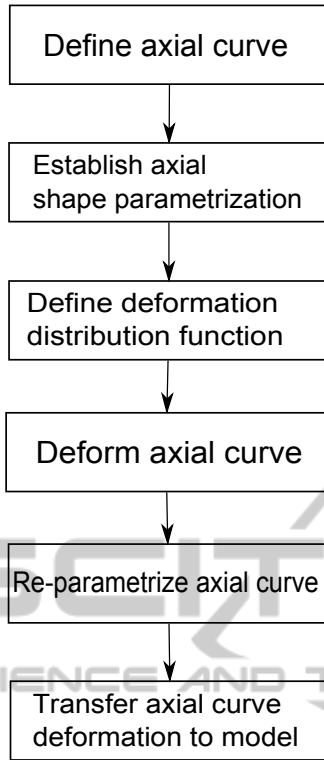


Figure 2: Flow chart of the proposed deformation method.

be found. Then, the local deformation  $\delta s(t)$  can be rewritten in terms of the given total deformation and bar's properties,

$$\delta s(t) = \delta L \frac{\int_0^t k^{-1}(t) dt}{\int_0^1 k^{-1}(t) dt}. \quad (4)$$

Let  $w(t) \in [0, 1]$  be the *deformation distribution function (DDF)* along the bar such that,

$$w(t) = \frac{\int_0^t k^{-1}(t) dt}{\int_0^1 k^{-1}(t) dt}. \quad (5)$$

Then Eq. (4) can be rewritten in a more compact form,

$$\delta s(t) = \delta L w(t). \quad (6)$$

For the uniform case when  $k(t) = \text{const}$ ,

$$w(t) = \frac{\int_0^t dt}{\int_0^1 dt} = t. \quad (7)$$

The local deformation  $\delta s(t)$  is then reduces to the uniform scaling,

$$\delta s(t) = \delta L t, t \in [0, 1]. \quad (8)$$

Similar results can be obtained for inhomogeneous bar under torsion (Timoshenko, 1970). By replacing the local stretching  $\delta s(t)$  with local rotation angle  $\delta \theta(t)$  and total length change with total rotation angle  $\delta \Theta$ , Eq. (6) can be rewritten as,

$$\delta \theta(t) = \delta \Theta w(t). \quad (9)$$

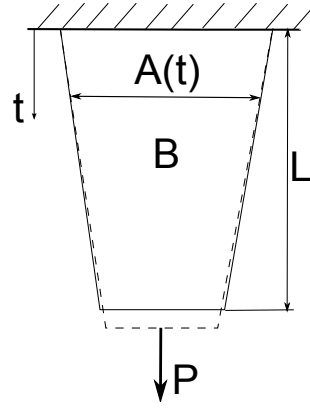


Figure 3: Bar with variable cross section under axial load.

## 2.2 Deformation Distribution Function

Function  $w(t)$  controls deformation distribution along the handle axis. With the proposed approach,  $w(t)$  is designed to avoid distortion of the important features of the model while obeying the boundary conditions imposed by the user. Kraevoy et al. (Kraevoy et al., 2008) estimate local *vulnerability* of the model to non-uniform scaling as a combination of slippage measure (Gelfand and Guibas, 2004) and normal curvature in the direction of deformation. Since in our case the deformation of the model  $M$  is guided by the axial curve  $C(t)$ , the proposed vulnerability measure is based on shape variation of  $M$  along  $C(t)$ . Assuming that length preserving bending does not introduce distortion as long as  $C(t)$  remains smooth, axial deformation can produce two types of distortion:

1. **Stretching:** by modifying the total length of  $C(t)$ .
2. **Torsion:** by imposing twist around the  $C(t)$ .

Stretching will not introduce any distortion in regions where the cross section of the model  $\chi_M(t)$  is constant along  $C(t)$ . Therefore, for regions with constant cross section the vulnerability to stretching  $v_{\delta L}(t)$  should be close to zero, and where cross section is rapidly changing,  $v_{\delta L}(t)$  should be high. In other words,  $v_{\delta L}(t)$  is proportional to the gradient of  $\chi_M(t)$  along  $C(t)$ ,

$$v_{\delta L}(t) \sim \|\nabla \chi_M(t)\| \quad (10)$$

On the other hand, torsion should be allowed where the shape contour is close to circular and prevented elsewhere to avoid distortion. So, the vulnerability to torsion  $v_{\delta \Theta}(t)$  can be estimated integrating the radius gradient across the shape profile  $\chi(t)$ ,

$$v_{\delta \Theta}(t) \sim \int_{\chi(t)} \|\nabla r_{\chi(t)}\|, \quad (11)$$

where  $r_{\chi(t)}$  is the local radius of the shape contour  $\chi(t)$ .

Replacing stiffness  $k(t)$  in Eq. (5) with the above vulnerability measures, deformation distribution functions (DDFs)  $w_{\delta L}(t)$  and  $w_{\delta\Theta}(t)$  can be formulated as,

$$w_{\delta L}(t) = \frac{\int_0^t v_{\delta L}(t) dt}{\int_0^1 v_{\delta L}(t) dt}, \quad (12)$$

$$w_{\delta\Theta}(t) = \frac{\int_0^t v_{\delta\Theta}(t) dt}{\int_0^1 v_{\delta\Theta}(t) dt}. \quad (13)$$

These functions are used to define weighted arc-length parametrization of the axial curve  $C(t)$  and to establish weighted rotation minimizing frame along  $C(t)$ .

### 2.3 Weighted Arc-length Parametrization

Arc-length preserving axial deformation produces natural results and therefore very useful in animation (Peng et al., 1997). However, when the length of the model is modified in purpose, arc-length of the axial curve  $C(t)$  cannot be preserved everywhere. However, it can be preserved *locally* by weighting the arc-length change with deformation distribution function (DDF)  $w_{\delta L}(t)$ .

The curve  $C(t)$  is initially parameterized w.r.t. its arc-length  $s(t)$  such that (do Carmo, 1976),

$$t = \frac{s(t)}{L}, t \in [0, 1], \quad (14)$$

where  $L$  is the total length of the curve. When  $L$  is modified by  $\delta L$ , the new parametrization  $\tilde{t}$  is computed as follows:

$$\tilde{t} = \frac{s(t) + \delta s(t)}{L + \delta L}, \quad (15)$$

where  $\delta s(t)$  is the weighted local deformation,

$$\delta s(t) = w_{\delta L}(t) \delta L. \quad (16)$$

This new parametrization is used to transfer the deformation of the axial curve  $C(t)$  to the model  $M$ , as will be explained in Section 2.5. As a result, the deformation  $\delta L$  is redistributed according to the DDF  $w_{\delta L}(t)$ .

### 2.4 Weighted Rotation Minimizing Frame

Establishing an appropriate frame field  $F(t) = (\mathbf{e}_1(t), \mathbf{e}_2(t), \mathbf{e}_3(t))$  is a basic task in curve design and analysis (Farin, 1997). While  $\mathbf{e}_3$  is usually associated with the tangent vector of the curve, another axis has

to be defined in order to set up the frame field completely. In differential geometry, the classical Frenet frame is commonly used,

$$(\mathbf{e}_1, \mathbf{e}_2, \mathbf{e}_3) \triangleq (\mathbf{n}, \mathbf{b}, \mathbf{t}), \quad (17)$$

where  $\mathbf{n}$ ,  $\mathbf{b}$  and  $\mathbf{t}$  are the normal, binormal and tangent respectively (Koenderink, 1990). The advantage of Frenet frame is that it can be computed analytically for any point on a twice differentiable curve. Unfortunately, for general curves with vanishing second derivative or high torsion, Frenet frame fails to generate stable well-behaving frame field. As a better alternative, Klok (Klok, 1986) introduced the rotation minimizing frame (RMF), which is formulated in differential form,

$$\mathbf{e}'_1 = -\frac{(C'' \cdot \mathbf{e}_1)C'}{\|C'\|^2}, \quad (18)$$

with initial condition  $\mathbf{e}_1(0) = \mathbf{e}_1^0$ . Although no analytic solution is available in that case, there is a simple and effective method to approximate RMF by discretizing the curve and propagating the first frame defined by the initial condition  $\mathbf{e}_1^0$  along the curve (Klok, 1986).

With additional boundary constraint  $\mathbf{e}_1(1) = \mathbf{e}_1^1$ , twist has to be introduced into the RMF (see Figure 4). The twisting angle  $\delta\Theta$  is then propagated along the axis according to the parameter  $t \in [0, 1]$ ,

$$\delta\theta(t) = \delta\Theta t. \quad (19)$$

The resulted frame field is shown in Figure 4(b).

As was already mentioned, imposing twist may distort certain features of the model. This effect is demonstrated in Figure 4(a). Using the proposed inhomogeneous approach, the twist  $\delta\theta(t)$  distribution will be adapted to the DDF  $w_{\delta\Theta}(t)$ ,

$$\delta\theta(t) = \delta\Theta w_{\delta\Theta}(t). \quad (20)$$

With this weighted torsion distribution, shown in Figure 4(d), the distortion of the features is avoided and applied in the invulnerable regions, as can be seen in Figure 4(c).

### 2.5 Model Embedding and Deformation Transfer

One of the important advantages of spatial deformation in general, and axial deformation in particular, is its independence of the deformed model  $M$  representation (Barr, 1984).  $M$ 's shape is assumed to be completely defined by position of finite set of control points  $P = \{\mathbf{p}_i(x, y, z), i = 0..n\}$ . For polygonal meshes,  $P$  is the list of the vertices, while for parametric surfaces,  $P$  will represent the control points.

The axial deformation consists of two mapping  $\mathbb{R}^3 \mapsto \mathbb{R}^3$  (Lazarus et al., 1994):

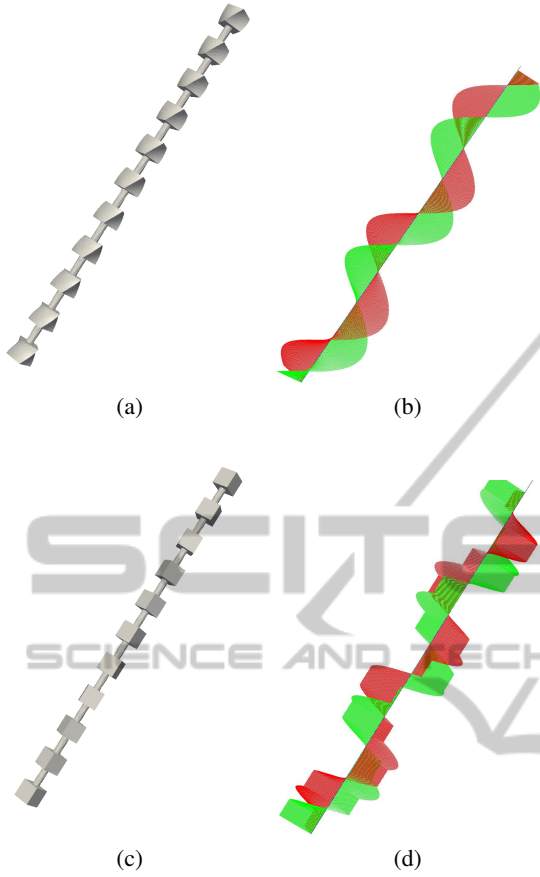


Figure 4: Comparison of Klok's RMF with the proposed weighted RMF: (a),(b) RMF creates distortion of the cubes, (c),(d) the proposed weighted RMF preserves the cubes while obeying the twist angle.

1. Embedding of the model  $M$  in parametric space of the axial curve  $C(t)$ .
2. Transfer of the deformation from  $C(t)$  to  $M$ .

To embed the model  $M$  in the parametric space, each control point  $\mathbf{p}_i \in M$  is equipped with triple  $(t_{\mathbf{p}_i}, \theta(t_{\mathbf{p}_i}), r(t_{\mathbf{p}_i}))$ , where  $t_{\mathbf{p}_i}$  is parameter of the handle axis  $C(t)$ ,  $\theta(t_{\mathbf{p}_i})$  is the rotation angle relative to the moving frame defined in Section 2.4, and  $r(t_{\mathbf{p}_i})$  is the distance between correspondent point  $C(t_{\mathbf{p}_i})$  and  $\mathbf{p}_i$  (see Figure 5).

Once  $M$  is embedded in the parametric space, deformation transfer from  $C(t)$  to  $M$  is straight forward,

$$\tilde{\mathbf{p}}_i = C(t_{\mathbf{p}_i}) + R(\theta_{\mathbf{p}_i})\mathbf{e}_1(t_{\mathbf{p}_i})r(t_{\mathbf{p}_i}), \quad (21)$$

where  $R(\theta_{\mathbf{p}_i})$  is the rotation matrix around axial curve. In some applications, it may be useful to introduce scaling in radial direction (Yoon and Kim, 2006). For example in Figure 1(d), uniform radial scaling is applied to compensate for stretching  $\delta L$ .

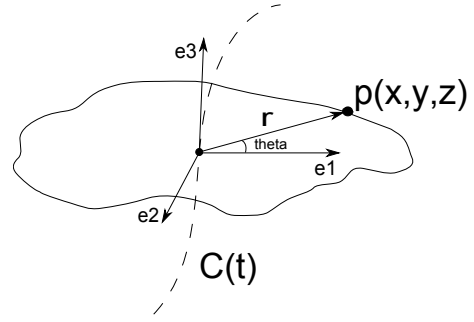


Figure 5: Axial parametrization of the model.

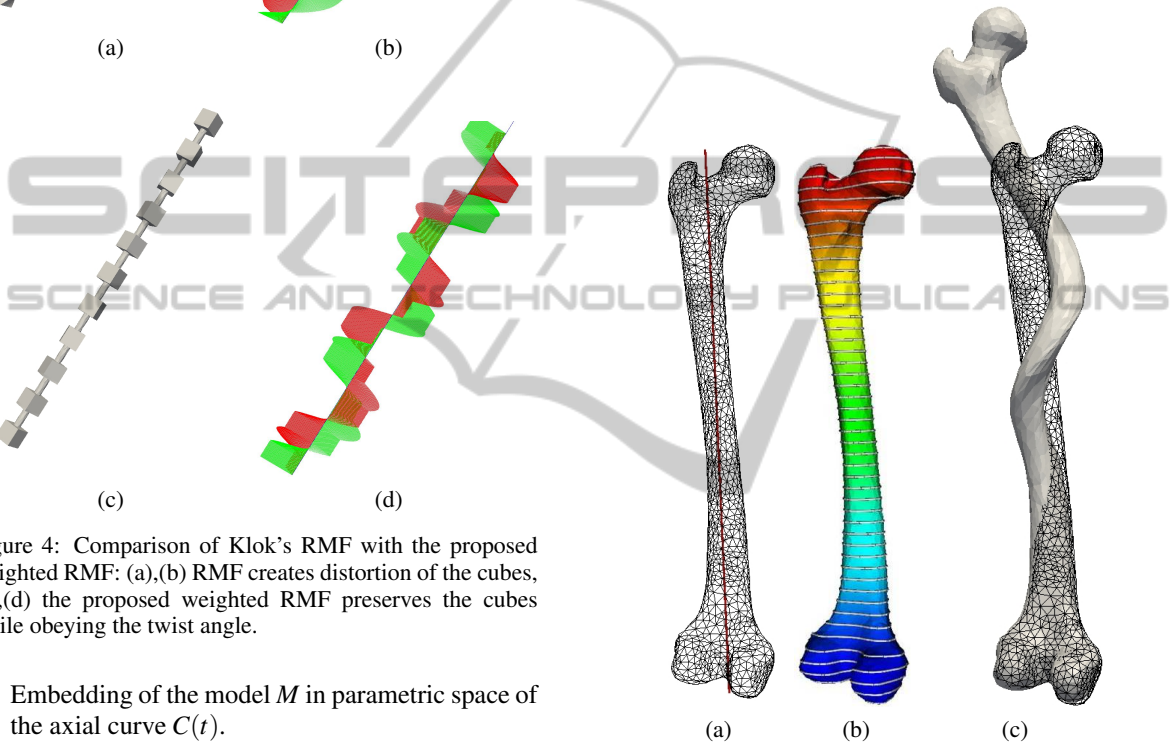


Figure 6: Femur model embedding and deformation: (a) handle axis initialized to the center line, (b) mesh vertices are parameterized along the center line and model profiles are extracted, (c) deformation transfer from the axis to the model; notice the shape preservation of the femoral head and the knee joint.

Then,  $r(t)$  is multiplied by a constant scaling factor,

$$\tilde{r}(t) = r(t) \frac{L + \delta L}{L}. \quad (22)$$

### 3 IMPLEMENTATION

The axial deformation session starts from setting the axial curve  $C(t)$  and associating control points  $P =$

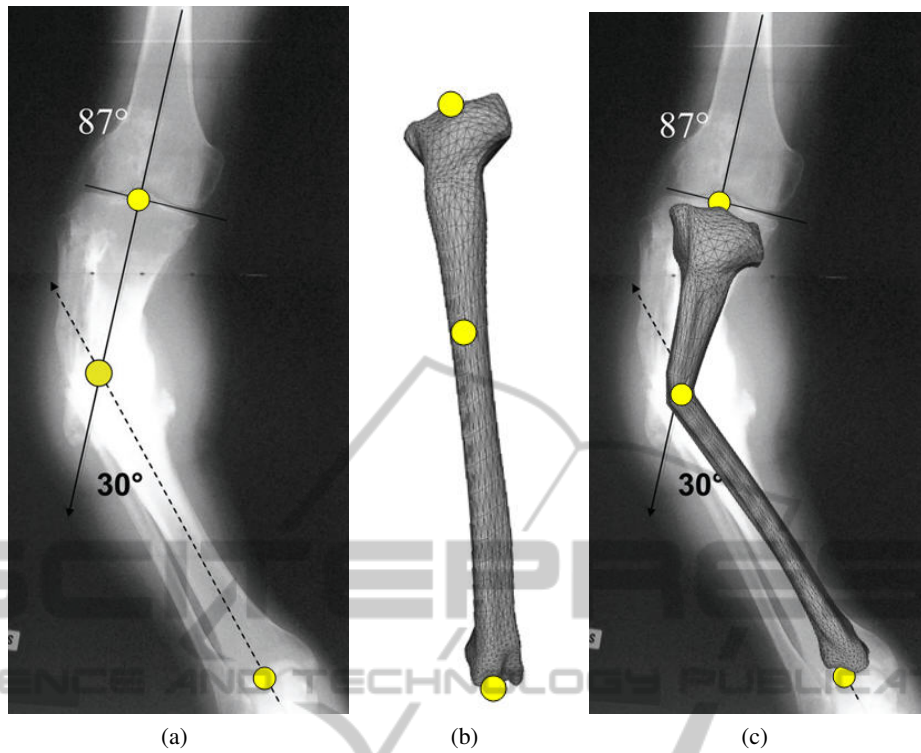


Figure 7: Tibia deformity modeling: (a) X-ray image of the tibia pathology, (b) template tibia model, and (c) overlay of the deformed 3D tibia on the 2D image.

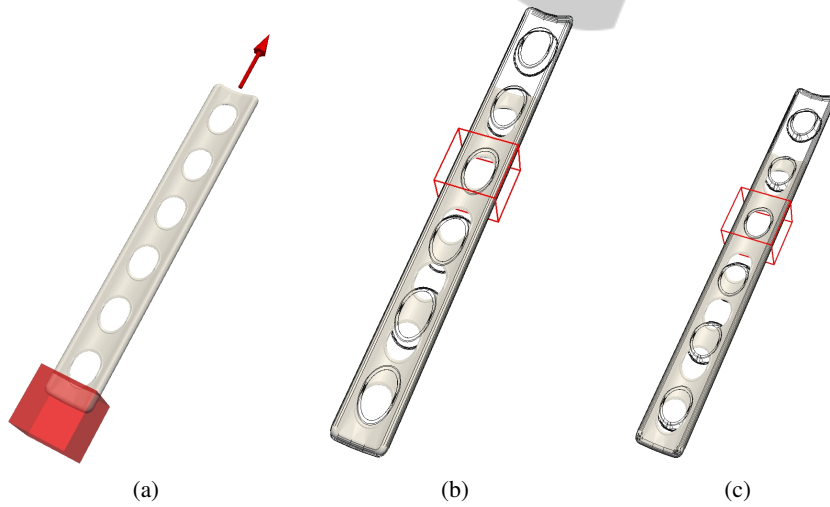


Figure 8: Plate deformation (original model is shown as solid and deformed as wire frame): (a) plate with shown boundary conditions, (b) after simple scaling holes are distorted, (c) with inhomogeneous deformation shape of the holes is preserved; notice the precise matching of the hole after deformation.

$\{\mathbf{p}_i, i = 1..n\}$  of the model  $M$  with this curve. First,  $M$  is oriented such that  $z$  axis is aligned with its maximal principal component. Afterwards,  $C(t)$  is initialized to the center line of  $M$ 's bounding box, as shown in Figure 6(a). Thus, parameter  $t_{p_i}$  of the control point

$\mathbf{p}_i$  can be directly computed from  $z_{p_i}$ ,

$$t_{p_i} = \frac{z_{p_i}}{z_{max} - z_{min}}. \quad (23)$$

These values are associated with each control point and stored. In addition, initial curve length  $L = z_{max} - z_{min}$  is stored.

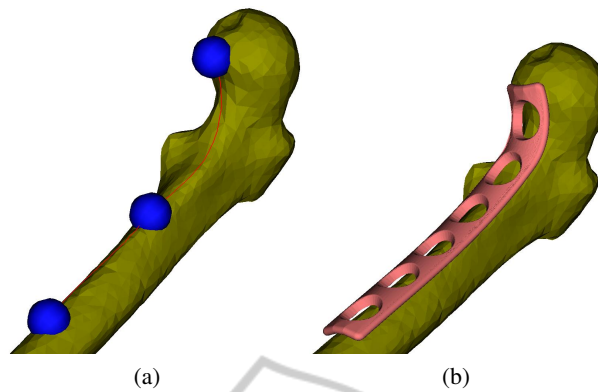


Figure 9: Semi-automatic implant placement on femur: (a) guiding points placed by the user, (b) appropriate plate is automatically picked from the implant database and deformed to fit the bone.

Afterwards, the model  $M$  is sliced with  $m$  planes perpendicular to the center line and the shape profiles are stored (see Figure 6(b)). Based on these profiles, vulnerability measures  $v_{\delta L}$  and  $v_{\delta\Theta}$  are estimated for each profile using Eqs. (10) (11). And DDFs  $w_{\delta L}$  and  $w_{\delta\Theta}$  are computed using Eq. (12) and stored.

When the axial curve  $C(t)$  is modified to  $\tilde{C}(t)$ , it is re-parameterized according to the new arc-length and the stored  $w_{\delta L}$  DDF using Eq. (15). If twist deformation is introduced, it is distributed according to the pre-computed  $w_{\delta\Theta}$  function.

For initially curved models it may be more intuitive to initialize  $C(t)$  to follow the shape of the model (Lazarus et al., 1994). One simple approach is to extract shape profiles parallel to some pre-defined plane and to fit  $C(t)$  to the centers of these profiles. In that case, several practical questions arise. First, for each control point  $\mathbf{p}$  closest point on  $C(t)$  has to be found, which may take significant computational effort for big models (Yoon and Kim, 2006). Second, models with complex topology (see for example model shown in Figure 8) may require special treatment in order to compute stable axial curve. Moreover, this simple approach may fail completely for certain models. In that case, a complete skeletonization should be applied (Au et al., 2008) and the resulting skeleton curve may be used as the deformation axis.

## 4 APPLICATIONS

The major motivation for this work came from bone modeling for orthopedic surgery planning. Currently, most interventions are still planned based on the pre-operative 2D X-ray images. Although significant amount of research work was dedicated to 3D orthopedic surgery planning (Hazan and Joskowicz, 2003),

it is assumed that pre-operative 3D image of the patient's anatomy is available. Unfortunately, this is not always the case. One way to overcome this issue is to recover 3D geometry from the available 2D data. This can be done by overlaying a template bone model on the image and deforming the model to approximate patient's pathology (Messmer et al., 2001). Figure 7 shows tibia deformity that is going to be treated with Ilizarov spatial frame (Rozbruch et al., 2006). In order to simulate this procedure, 3D tibia model is deformed to match the available 2D image using the proposed inhomogeneous AxDf approach. With this approach, tibia features can be automatically preserved during the deformation, without explicit user specified constraints, as can be seen in Figure 7.

Due to its feature preserving property, the proposed approach is also used for implant modeling for pre-operative planning of fracture reduction and fixation. Figure 8 shows how shape of the implant holes is preserved under axial load with the proposed inhomogeneous axial deformation method. This is important since distortion of the holes will make it difficult or impossible insertion of the fixation screws. Fracture care systems that are currently in clinical use perform planning in 2D and require manual reduction of the fracture and fitting of the implant to the bone. With the proposed semi-automatic implant placement, the surgeon just needs to mark region on the bone where the implant should be placed. Then, the system will automatically adapt the implant's shape and size to the bone, as shown in Figure 9. This is achieved by computing implant path on the bone from the provided guiding points using the shortest-path algorithm (Surazhsky et al., 2005). From the computed path, appropriate plate length is estimated and the appropriate plate is chosen automatically from the implant database. Finally, the chosen plate is deformed preserving shape of the holes, while the path is used

as the deformation axis.

## 5 CONCLUSIONS AND FUTURE WORK

In this paper, inhomogeneous axial deformation was introduced and demonstrated on a number of important applications in orthopedic surgery planning. The proposed method inherits all the attractive properties of the classical axial deformation and introduces shape sensitivity to the original formulation. This allows to preserve shape and size of the features while reducing required user interaction.

Currently, only shape of the model is used for the DDF formulation. However, physical material properties can be easily incorporated into the proposed framework.

Another promising research direction is learning of deformation modes from provided examples (Popa et al., 2006). This would allow intelligent adaptation of the deformation distribution functions to the specific domain.

By definition, AxDf supports a limited class of deformations. The proposed approach can be extended to handle more general deformation schemes. In particular, it would be interesting to combine the proposed inhomogeneous formulation with the sweep-based freeform deformation method (Yoon and Kim, 2006). It is also possible to formulate two-dimensional DDFs to consider deformations guided by parametric surfaces (Feng et al., 1996).

## REFERENCES

- Au, O. K.-C., Tai, C.-L., Chu, H.-K., Cohen-Or, D., and Lee, T.-Y. (2008). Skeleton extraction by mesh contraction. *ACM Trans. Graph.*, 27:1–10.
- Azernikov, S. (2008). Sweeping solids on manifolds. In Haines, E. and McGuire, M., editors, *Symposium on Solid and Physical Modeling*, pages 249–255. ACM.
- Barr, A. H. (1984). Global and local deformations of solid primitives. In *ACM Computer Graphics SIGGRAPH '84*, pages 21–30.
- do Carmo, M. P. (1976). *Differential Geometry of Curves and Surfaces*. Prentice-Hall, Inc.
- Farin, G. (1997). *Curves and Surfaces for Computer-Aided Geometric Design - A Practical Guide*. Academic Press.
- Feng, J., Ma, L., and Peng, Q. (1996). A new free-form deformation through the control of parametric surfaces. *Computers & Graphics*, 20(4):531–539.
- Gain, J. E. and Bechmann, D. (2008). A survey of spatial deformation from a user-centered perspective. *ACM Trans. Graph.*, 27(4).
- Gelfand, N. and Guibas, L. J. (2004). Shape segmentation using local slippage analysis. In Fellner, D. and Spencer, S., editors, *Proceedings of the 2004 Eurographics/ACM SIGGRAPH Symposium on Geometry Processing (SGP-04)*, pages 219–228, Aire-la-Ville, Switzerland. Eurographics Association.
- Hazan, E. and Joskowicz, L. (2003). Computer-assisted image-guided intramedullary nailing of femoral shaft fractures. *Techniques in Orthopedics*, 18(2).
- Klok, F. (1986). Two moving coordinate frames for sweeping along a 3D, trajectory. *Computer Aided Geometric Design*, 3(3):217–229.
- Koenderink, J. J. (1990). *Solid Shape*. MIT Press.
- Kraevoy, V., Sheffer, A., Shamir, A., and Cohen-Or, D. (2008). Non-homogeneous resizing of complex models. *ACM Trans. Graph.*, 27(5):111.
- Lazarus, F., Coquillart, S., and Jancène, P. (1994). Axial deformations: an intuitive deformation technique. *Computer-Aided Design*, 26(8):607–613.
- Lipman, Y., Sorkine, O., Levin, D., and Cohen-Or, D. (2005). Linear rotation-invariant coordinates for meshes. *ACM Transactions on Graphics*, 24(3):479–487.
- Messmer, P., Long, G., Suhm, N., Regazzoni, P., and Jacob, A. (2001). Volumetric model determination of the tibia based on radiographs using 2d/3d database. *Computer Aided Surgery*, 6:183–194.
- Peng, Q., Jin, X., and Feng, J. (1997). Arc-length-based axial deformation and length preserved animation. IEEE Computer Society.
- Popa, T., Julius, D., and Sheffer, A. (2006). Material-aware mesh deformations. In *Shape Modeling International*. IEEE Computer Society.
- Rozbruch, S. R., Fragomen, A. T., and Ilizarov, S. (2006). Correction of tibial deformity with use of the ilizarov-taylor spatial frame. *Journal of Bone and Joint Surgery*, 88:156–174.
- Sederberg, T. W. and Parry, S. R. (1986). Free-form deformation of solid geometric models. In Evans, D. C. and Athay, R. J., editors, *Computer Graphics (SIGGRAPH '86 Proceedings)*, volume 20, pages 151–160, Dallas, Texas.
- Sorkine, O. (2005). Laplacian mesh processing. In Chrysanthou, Y. and Magnor, M., editors, *STAR Proceedings of Eurographics 2005*, pages 53–70, Dublin, Ireland. Eurographics Association.
- Surazhsky, V., Surazhsky, T., Kirsanov, D., Gortler, S. J., and Hoppe, H. (2005). Fast exact and approximate geodesics on meshes. *ACM Trans. Graph.*, 24:553–560.
- Timoshenko, S. (1970). *Theory of Elasticity*. McGraw Hill.
- Yoon, S.-H. and Kim, M.-S. (2006). Sweep-based freeform deformations. *Computer Graphics Forum*, 25(3):487–496.